Applied Surface Science 562 (2021) 150167

Contents lists available at ScienceDirect

Applied Surface Science

journal homepage: www.elsevier.com/locate/apsusc

Full Length Article

Impact of deposition conditions on nanostructured anisotropic silica thin films in multilayer interference coatings

Lina Grineviciute [a,*], Holger Badorreck [b,c], Lars Jensen [b,c], Detlev Ristau [b,c,d], Marco Jupé [b,c], Algirdas Selskis [a], Tomas Tolenis [a]

[a] Center for Physical Sciences and Technology, Savanoriu Ave. 231, LT-02300 Vilnius, Lithuania
[b] Laser Zentrum Hannover e.V., Hollerithallee 8, Hanover, Germany
[c] PhoenixD, Leibniz University Hanover, Germany
[d] Institute of Quantum Optics, Leibniz University Hanover, Germany

ARTICLE INFO

Keywords:
Sculptured thin films
Anisotropic coatings
Phase retardance
Effective refractive index
Surface filling
Molecular dynamics

ABSTRACT

Recent developments of nanostructured coatings have reached a point where extensive investigations within multi-layer systems are necessary for further implementation in novel photonic systems. Although sculptured thin films are explored for decades, no optical and structural measurements have been performed for anisotropic nanostructured multi-layer coatings with different deposition conditions of the dense layer. In this paper, we present extensive morphological analysis on silica nanostructured anisotropic films. Changing the deposition angle from 66° to 84°, indicate the changes in surface filling from 84% to 57%, respectively, while phase retardance has a maximal value of 0.032°/nm at 70° and 72° angles. We also present the investigation of covering such structures with the dense layer at different conditions. As a result, the technology for maintaining initial anisotropic properties is developed for extending spectral difference 1.6 times and phase retardation by 5% in anisotropic multi-layer coatings. Furthermore, we present simulations of growing silica layer using experimental conditions in the Virtual Coater framework resulting in virtual anisotropic films for comparison with measurements. The minimal impact on the anisotropy of porous layer is reached with the deposition of dense layer at 30° angle during constant substrate rotation.

1. Introduction

Advancements in nano-engineered coatings have extended the applications of thin films in virtually every topic. Telecommunications have benefitted from bottom-up surface modification techniques in many aspects [1]. Photovoltaics partly became the science of thin films and surface modification methods [2]. Optics and photonics also have their significant share in the usage of thin film technologies, mostly in optical coatings applications [3].

The GLancing Angle Deposition method (GLAD), which has been under constant development for more than 30 years, introduced the flexibility in thin films morphology. Based on self-shadowing effects, GLAD is capable to form nano-engineered coatings with slanted or vertical columnar, zig-zag [4], chiral [5,6], etc. nano-structures. Together with morphological changes, the characteristics of the films (optical properties, porosity, etc.) are also affected and used in developing advanced elements. A main example would be optical coatings, where the effective refractive index and even its birefringence can be controlled by changing the orientation of the substrate with regards to the vapor flux. Such developments have led to new types of optical components, e.g. coating-based waveplates [7,8], advanced anti-reflection coatings [9,10], Bragg mirrors with selectivity of circular polarization [11], polarization-active Bragg microcavities acting as wavelength retarders [12], etc. Combination of such nano-structures with liquid infiltration even allowed the development of switchable radial polarization converters based on sculptured thin films [13,14].

Recently, GLAD technology has been extended by combining nano-structured layers with dense thin films, resulting in even more complex multi-layer coatings. Changing the orientation of the substrate and the porosity, as a result, allows to obtain discrete layers with different optical properties using the same raw material. Major examples have been published during the last several years: all-silica anti-reflection coatings [9,10], mirrors [15], and waveplates [10,16]. All three components have demonstrated their extreme resistivity to laser radiation.

* Corresponding author.
E-mail address: lina.grineviciute@ftmc.lt (L. Grineviciute).

https://doi.org/10.1016/j.apsusc.2021.150167
Received 21 January 2021; Received in revised form 5 May 2021; Accepted 17 May 2021
Available online 23 May 2021

Despite the advanced properties of all-silica multi-layer coatings, new issues have appeared within the GLAD method. During the deposition of porous/dense layers, structural inhomogeneities lead to spectral errors and limitations for complex coating designs. This paper addresses these issues by extensively investigating 2-layer systems of silica formed by GLAD: Firstly, a nanostructured anisotropic layer, and secondly, this same layer with a dense layer on top. A modified sequence in the formation of multi-layer anisotropic coatings is presented.

The paper is divided as follows: section 2 describes experimental materials and methods; section 3 describes the results of detailed investigations of single- and multi-layer anisotropic layers; section 4 describes theoretical simulations of 2-layer systems and offers an interpretation of the interface evolution.

2. Materials and methods

An electron beam evaporation technique ("SIDRABE", Latvia) was used for all silica thin films deposition processes. Fused silica (FS) glasses with a diameter of 25.4 mm and Si plates were used as substrates. SiO_2 granules (Umicore) were used as evaporation source in each process. The distance between substrate and evaporation source is 34 cm. During the process, the layer growth rate was controlled with a crystal quartz monitor and maintained at 3 Å/s. Depositions were started at room temperature in a vacuum chamber at the pressure of 1.5×10^{-3} Pa. During the evaporation process, 2 sccm (the partial pressure of $2 \cdot 10^{-4}$ mbar) of oxygen gas was introduced into the chamber to ensure the oxidation of any non-oxidised particles in vapor flux.

A birefringent layer is obtained using one particular GLAD method – serial bi-deposition (SBD) [17]. During this process, the substrate was set at an oblique angle χ and rotated in half-turns (axial rotation α) around the surface normal without stopping the deposition process. The constant time period of half turns ($\alpha = 180°$) was induced in order to form structures, similar to chevrons, with 1–2 nm thickness sub-deposits (see Fig. 1). In this investigation, samples were coated by setting the angle χ to 66, 70, 72, 74, 76, 78, 80, and 84°and also various 2-layers, and 6-layer structures were fabricated and analyzed in detail by scanning electron microscopy (SEM), spectrophotometry and ellipsometry.

Transmission and phase delay difference between two perpendicular linear polarizations, namely in the shadowing plane (fast axis) and perpendicular to it (slow axis), are measured by a spectrophotometer ("Photon RT", Belarus) and spectrophotometric ellipsometer ("J. A. Woolam RC2", USA), respectively. The retardance difference is obtained by aligning the shadowing plane with one of the ellipsometry axes and then directly measuring the phase delay difference in transmission mode at 0° angle of incidence. The dispersions of the refractive indices of silica thin films were modeled by using the "Optilayer" software [18] and fitting transmission spectra (see Fig. 3(a)).

3. Results

Experimental research is divided into two parts: analysis of single- and multi-layers. The first part describes the optical and structural properties of anisotropic thin films deposited at different angles. The second part includes the detailed analysis of multi-layer structures, which are formed considering the results of the previous investigation.

3.1. Single-layers

A detailed investigation of optical and structural properties has been performed for anisotropic silica single-layers in order to determine the optimal deposition parameters to reach the highest anisotropy within the film. When increasing the deposition angle, the influence of the self-shadowing effect increases, which leads to more porous layer formation and, therefore in a lower effective refractive index of the film. Because the shadowing effect mostly dominates in one direction, when looking from the top, such structured layers indicate elliptical shape columns (see insert in Fig. 1). Therefore, optical anisotropy appears with a slow and a fast axis as in crystals with natural anisotropy, which allows the birefringent layer formation. Due to this SBD process the porosity increases differently in perpendicular directions and induces the formation of open cracks what is known as the bundling effect [12,19]. Since during low energy deposition, the surface morphology of the layer is the main factor for the formation of the secondary film, SEM images have been analyzed for the nanostructured thin films with thicknesses of 250 nm, deposited at different angles. The surface filling as a function of the deposition angle is presented in Fig. 2. The analysis indicates a continuous decrease of the surface filling when depositing at larger angles. Open pores strongly influence the deposition on top of such surfaces. This cannot only change the morphology of the secondary layer but can affect the first one as well.

Deposition at larger angles changes not only the nanostructure of thin films, but optical properties as well. Gradually increasing the deposition angle between the vapor flux and the substrate normally reduces the effective refractive index values due to an increasing self-shadowing effect, and therefore the porosity. Since the shadowing effect occurs only in one direction, the birefringence of silica films also depends on the deposition angle. Difference in refractive indices, for the thin film deposited at 70° angle, is lower compared to Smith et al. [20] and equals 0.028 at the wavelength of 350 nm. Difference can be influenced by humidity during the measurements and modelling of the spectra. SiO_2 anisotropic thin films exhibited the highest phase retardance of 0.032°/nm at the deposition angles of 70° and 72°. Similar

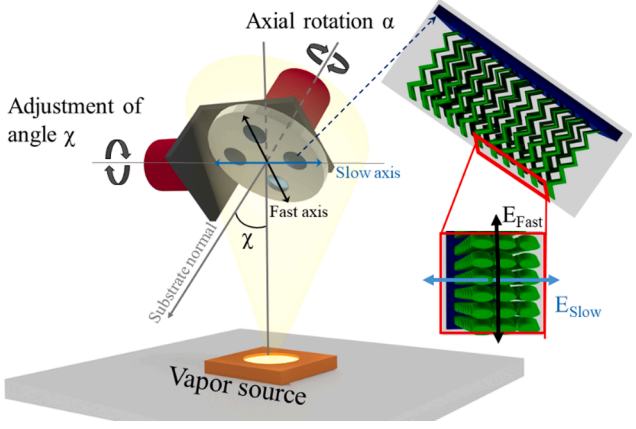

Fig. 1. The principal scheme of oblique angle deposition. χ indicates the angle between the vapor flux and the normal of the substrate surface.

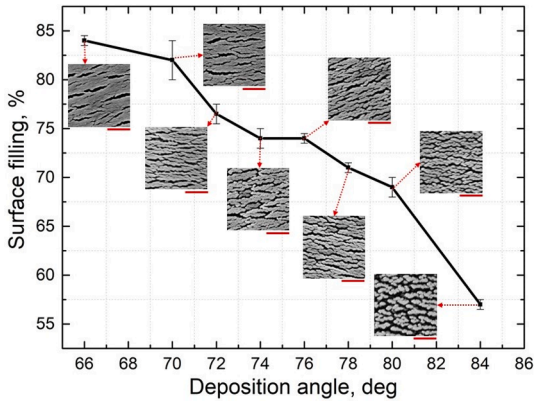

Fig. 2. Surface filling and SEM images of single layer anisotropic coatings (top view) deposited at different angles (Red bar under each SEM image is set at 500 nm). (For interpretation of the references to colour in this figure legend, the reader is referred to the web version of this article.)

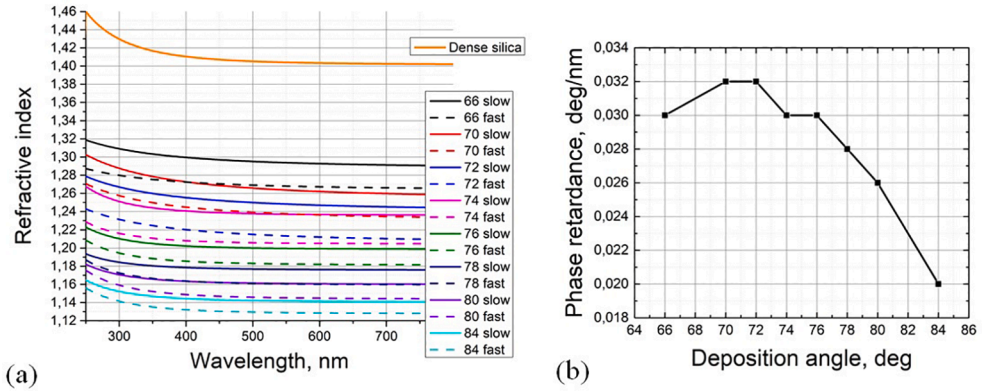

Fig. 3. (a) Refractive index dispersions of SiO_2 layers evaporated at different angles. slow axis - polarization perpendicular to shadowing direction, fast – polarization parallel to shadowing direction and (b) phase retardance of SiO_2 single layers evaporated at different angles.

tendencies were reported in other scientific publications, which were conducted for sculptured films made from materials like Ta_2O_5, WO_3 and Bi_2O_3 [7]. As stated above, optical analysis indicates that two deposition angles, namely 70° and 72°, are the most effective for the formation of anisotropic coatings, waveplates in our case. Additionally, surface structural investigations show (in Fig. 2) that thin films deposited at an angle of 70° have a higher filling factor of 5.5% compared to thin films deposited at 72° angle. This is preferable for multi-layer elements and for gaining better environmental stability due to less open areas within the coating, which can be exposed to contamination.

A deposition at 70°was chosen for further analysis as an optimal angle. Due to the competitive growth between fractions in the nanostructured layer, the expansion and coalescence of columns are present during the film growth [8]. The evolution of the film surface and optical anisotropy with increasing film thickness is shown in Fig. 4. The birefringence is influenced and changes with the thickness of the layer. Additionally, the increased size of the features can cause some negative side effects, such as optical scattering.

The surface analysis from SEM images indicates the decreasing surface filling of the films and the formation of wider cracks by increasing the film thickness, possibly due to the coalescence of the columns. The surface filling has decreased from 83.5% to 70% when the thickness of the film changed from 50 nm to 1500 nm, respectively. The mean area of the individual cracks has also increased from 86 nm^2 to 396 nm^2, accordingly. We can also observe from SEM images that cracks are increasing in both directions: fast and slow axis. After approximation of the elliptic form to each of the crack (please see Supplementary file), an increase of the largest minor axis within the surface of the film was determined: it changed from 20 nm to 81 nm when the thickness of the film changed from 50 nm to 1500 nm, respectively. Due to this structural gradient in the thin film growth axis, the optical anisotropy is affected as well. We can see the inhomogeneity of the normalized phase retardance dispersions of single layers with different thicknesses in Fig. 4(b). The phase retardation value at 350 nm wavelength for the film of 50 nm thickness is 0.025 °/nm. It increases 1.30 and 1.54 times when thickness increases to 400 nm and 1500 nm, respectively. According to our previous investigations of SiO_2, Al_2O_3, and LaF_3 nanostructured thin films, the cross-section of the plane perpendicular to the shadowing direction in the silica layers consists of columnar structures with gradually increasing diameters of individual columns as the film grows [8]. At the beginning of the film growth, the average widths of the columns are equal to ~29 nm. When film thickness reaches 400 nm, the coalescence of columns has started, and the width of the individual element extends to ~31 nm. Near the top of the layer (1.5 μm thickness), the width of the structural element increases to 70 nm. The expansion and later the coalescence of such columns leads to film inhomogeneity and light scattering for shorter wavelengths. Average phase retardation is similar in thin films with thicknesses from 200 nm to 400 nm. Layers of larger thickness are limited in quality and precision for coatings due to (i) inhomogeneous optical properties, (ii) optical scattering, (iii) wider crack formation, and (iv) mechanical instability. A multi-layer approach, i.e., the combination of porous anisotropic thin films with dense layers, has already been proven as a viable solution. Unfortunately, the deposition at close to normal incidence for dense thin film

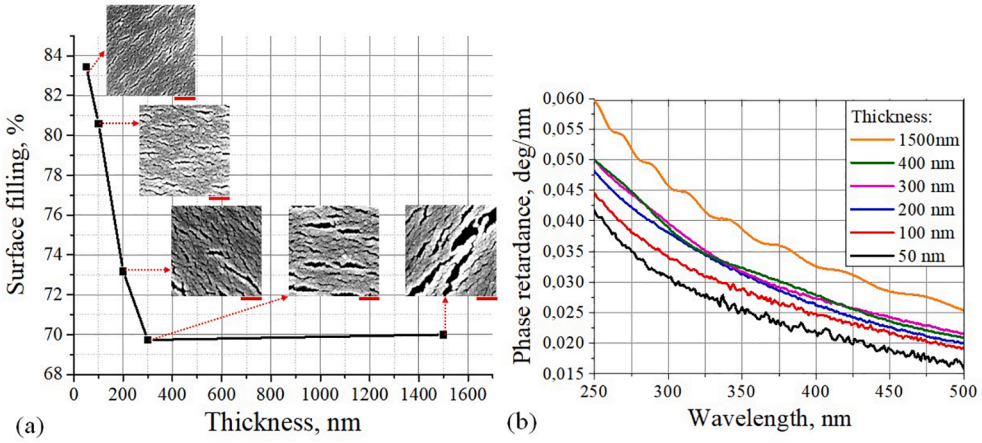

Fig. 4. The analysis of single-layer anisotropic coatings deposited at 70° angle by SBD method with different thicknesses. (a) Surface filling dependency on film thickness together with top-view SEM images (red bar under each SEM image is set at 200 nm), (b) normalized phase retardance. (For interpretation of the references to colour in this figure legend, the reader is referred to the web version of this article.)

formation still is highly influenced by larger voids in the porous layer. This can lead to larger inhomogeneities, therefore must be addressed.

3.2. Multi-layers

The combination of porous and dense layers with different inner structures allows to the creation of an interference coating using only one material. As it is shown in Fig. 3, depending on the deposition parameters, the same material can exhibit different effective refractive indices in a wide range (in case of SiO_2 from 1.41 to 1.13). Tailoring the nanostructures for individual layers induces Fresnel reflections in multi-layer coatings due to the difference in refractive indices, and therefore, various optical designs can be realized. For designs, which require high precision of optical properties, the combination of porous and dense layers must be controlled with high precision; therefore the investigation of the interface is crucial.

As the first step of multi-layer analysis, the 2-layer structures are fabricated and investigated in detail. The first layer (the base) is deposited at 70° angle with a thickness of 250 nm and is kept the same in all 2-layer coating experiments (see Fig. 5). The second layer is deposited with changed GLAD conditions: different deposition angles of incidence (χ) or different vapor flux directions. For three samples, a second layer with a thickness of 50 nm is deposited using constant rotation around the substrate axis and setting χ at 0, 30, and 50°. For the fourth sample, the second layer is deposited by the SBD method with an angle of $\chi = 50°$ and a time delay of 6 s between the half-rotations is maintained.

The qualitative SEM analysis was performed by combining cross-sections and top imaged to 3D images for the base layer and all 2-layer coating samples (Fig. 6). As it can be seen in Fig. 6(a), the base anisotropic layer surface structure consists of open cracks. As the second layer is being deposited on such base structure, some of the particles are penetrating inside the open voids and influence the optical properties of the first layer, therefore generating a transition zone. Furthermore, it is required for the dense layer to close the voids and to serve as a solid base for the next porous layer deposition. Depositing the secondary film at 0° and 30° closes most of the cracks (Fig. 6(b) and (c)), and it can be considered as a dense layer. Deposition at larger angles, 50° in our case, maintains open cracks and cannot be considered as a dense film for the multi-layer structure. Original SEM images of cross-sections of slow and fast axis can be found in Supplements Figs. S4 and S5.

Atomic Force Microscopy (AFM) measurements of surface roughness indicate that deposition at normal incidence also provides the lowest RMS values of 1.28 nm (Fig. 7(b)) in the experiment. Smooth surfaces after dense film deposition allow maintaining similar conditions in the growth of further porous anisotropic films and throughout all multi-layer formation. Depositions at 50° using constant substrate rotation or implementing SBD result in surfaces with open cracks and increased roughness of 1.60 nm and 1.68 nm, respectively. The comparison of the structural analysis between all 2-layers coatings indicates that only depositions at 0° and 30° angles are viable for the multi-layer formation and must be investigated further in order to determine their optical performance.

In order to enhance the spectral response to the multi-layer, consisting of nanostructured porous and dense layers, additionally, two 6-layer coatings were deposited. The anisotropic layers were the same in both designs, but the dense layers were deposited with constant rotation at different angles (0° and 30°), shown in Fig. 8(a). Both coatings are measured with the spectrophotometer and the ellipsometer (see Fig. 8 (b) and (c), respectively) for transmittance and phase retardance analysis. The multi-layer structure, which contains a dense layer deposited at a normal angle, exhibited a spectral difference in transmission of 3.9 nm (see Fig. 8(b)). For the dense layer deposited at 30° incidence, the spectral difference extended 1.6 times to 6.2 nm, indicating a larger optical anisotropy in the multi-layer coating. Additionally, the phase retardance is also evaluated for both experimental samples (see Fig. 8 (c)). The multi-layer, which contains layers deposited at 30°, exhibits a larger phase retardance value by ~5% throughout all UV spectra. Since dense films, deposited at both angles, are formed using constant substrate rotation, no birefringence is expected when light is irradiated at a normal angle. Therefore, phase retardance and spectral difference are present only due to the anisotropic layers, which are deposited at the same conditions in both cases. The difference in both optical properties, intensity and phase retardance, can be explained by considering the larger open cracks in anisotropic films surface. Deposition at a normal angle has a lower shadowing effect comparing to deposition at an incidence of 30°. Therefore, some part of the initial vapor flux can travel deeply into the pores and condensate in the initial film, and reduce its anisotropic properties. The transmission spectra of the multi-layer coating, deposited using 30° angle for dense films, is also shifted to the shorter wavelengths and has lower reflectance values near the Bragg zone. This behavior coincides with the multi-layer structure, which has lower refractive indices and a smaller difference between them. The refractive index of the dense film is slightly larger when deposited at 0° angle compared to the index of the film deposited at 30° angle. Therefore, the spectral changes of the Bragg zones depth are attributed to the reduced index of dense layers. The increased spectral difference of the Bragg zone for perpendicular polarizations is attributed to the larger anisotropy of the films deposited at 30° angle (when dense layers are deposited at 30° angles). Deposition of dense layers at 0° angle results in densifying the porous layer and reducing its anisotropy compared to the deposition of a dense thin film at 30° angle. In order to confirm this hypothesis, the growth of the coating was simulated and analyzed.

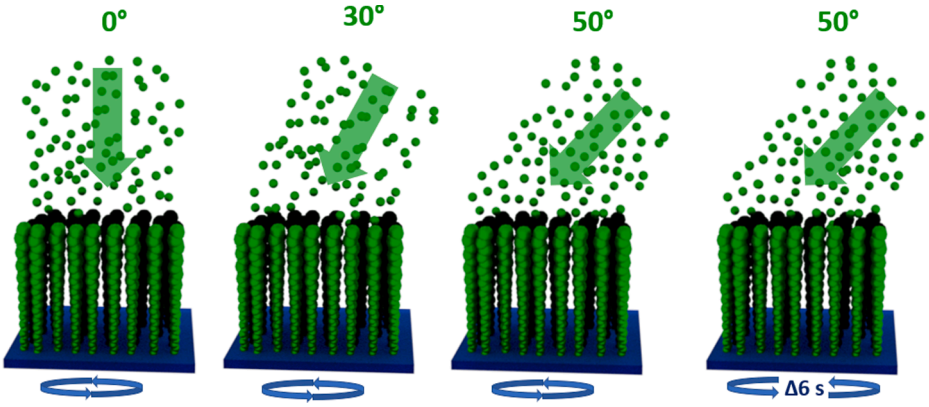

Fig. 5. The schematic representation of deposition conditions to form the second (dense) layer.

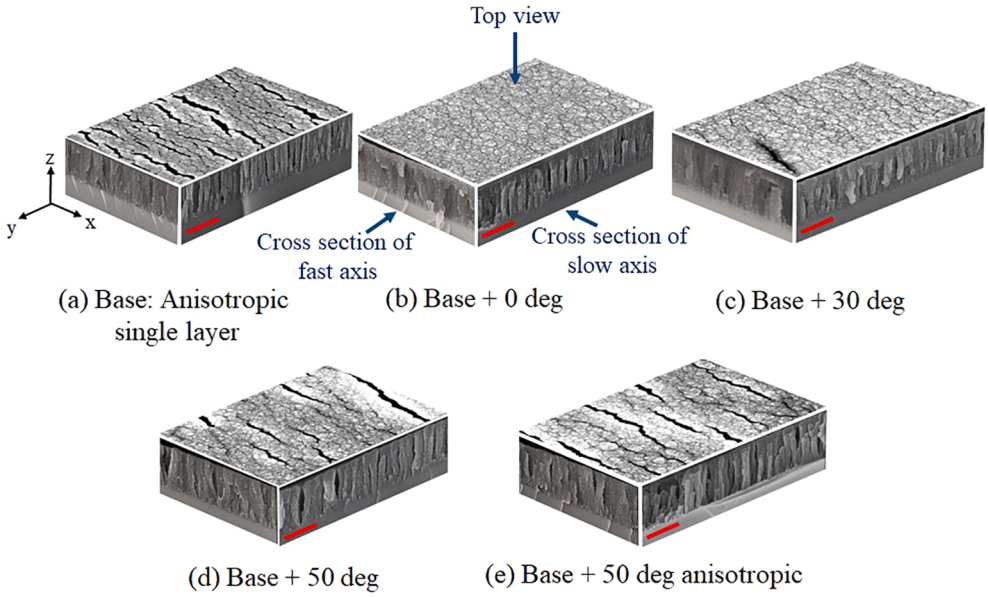

Fig. 6. 3D representation of SEM images combination of (a) single layer with 250 nm thickness, deposited at an angle of 70° and 2-layers structures with the second layer deposited at (b) 0°, (c) 30, (d) 50° and (e) 50°-anisotropic case. Red bar for each combination of SEM images is set at 250 nm. All structures are aligned the same way. Slow axis is parallel to *y* direction, fast axis is parallel to x direction. (For interpretation of the references to colour in this figure legend, the reader is referred to the web version of this article.)

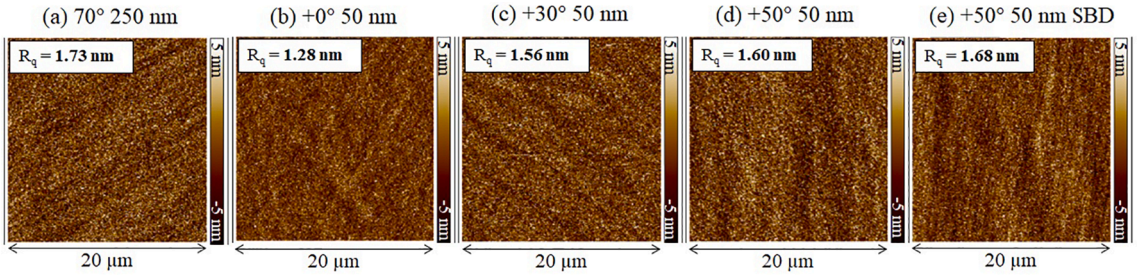

Fig. 7. AFM images of base single-layer (a) and 2-layer structures with top layer deposited at (b) 0°, (c) 30°, (d) 50°, and (e) 50° (anisotropic case).

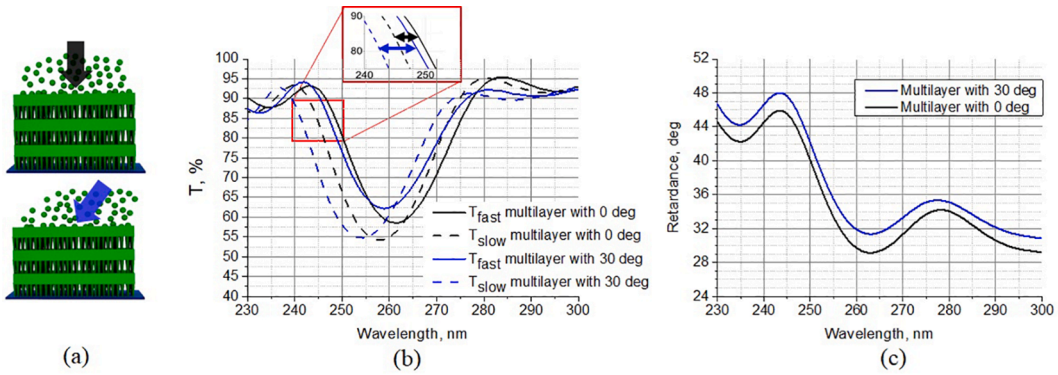

Fig. 8. (a) The schematic representation of a multi-layer structure with dense layers deposited at different angles, (b) transmission spectra of fabricated multi-layers for perpendicular polarizations (slow and fast axis), (c) the normalized retardance of fabricated multi-layer.

4. Atomistic thin film growth - molecular dynamics (MD)

For the growth simulation of SiO_2 multi-layers of anisotropic and dense films, the interaction potential from Zhang et al. [21] is used for the classical molecular dynamics (MD) performed with LAMMPS [22,23]. The simulation is performed for a substrate area size of x = 16 nm and y = 7 nm with lateral periodic boundary conditions. The first layer simulates a SBD coating (Fig. 9(a)) under an angle of $\chi = 70°$, where the angle α is flipped by 180° for every 1.5 nm of structure height (i.e., mean of the structure surface). The structure shown in Fig. 9(a) is grown with 10 flips of α. As deposition energy 0.3 eV is used throughout the simulation for silicon, while oxygen is deposited with no energy, i.e. it is adsorbed only in case of an attractive local potential on the surface. This method for oxygen serves as a simplified simulation of the common process of saturation in physical vapor deposition (PVD). For the purpose of simplicity, the deposition of more complex particles, like SiO_2 molecules, is only considered by the ratio between silicon and oxygen. The continuation on top of the zig-zag structure is done with more dense layers, deposited with an incidence of $\chi = 0°$, 30° and 50° in Fig. 9(b)–(d) during rotation of the structure by the azimuth angle α. The rotating

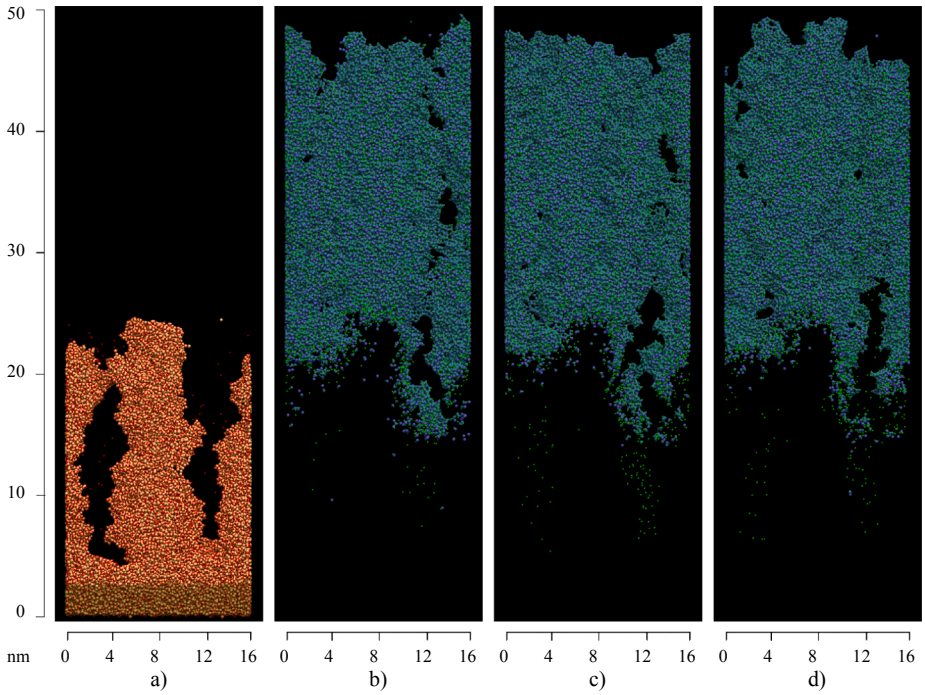

Fig. 9. Side view of simulated coatings (y-axis normal to paper plane), (a) the initial 1-layer zig-zag structure grown like SBD (red-yellow) with the substrate indicated by the shadowed area. The 2-layer structures with the second layer in blue-green continuing the first layer (not shown here) with different incidence angles χ during rotation of the azimuth α. (b) $\chi = 0°$, (c) $\chi = 30°$, (d) $\chi = 50°$. The filling of surface pores of the first layer is more pronounced for smaller angles χ. Graphics are generated with VMD [24]. (For interpretation of the references to colour in this figure legend, the reader is referred to the web version of this article.)

speed is 2.5 turns/nm.

Therefore, these simulations represent the digital twin of the experimental coatings shown in Fig. 6(a)–(d). As can be seen from Fig. 9 (a), the zig-zag layer exhibits a columnar structure. Although the simulation yields only two columns here due to the limited structure size and taking the periodic boundary into account, two major effects can already be observed. That is the beginning coalescence on the left side, while on the right an open pore and crack are build up. However, because the coalescence is not reproduced fully here, the columns widths are much smaller than observed in the experiment. With the continuation in Fig. 9(b)–(d), the closed pore on the left of each structure is nearly unchanged. In contrast, the open pore on the right is filled with additional material, which even leads to a closed small pore for 0°, while the impact on the initial layer decreases with increasing deposition angle as shown in Fig. 9(c) and (d). However, the second layer qualitatively changes the structure morphology, including only pores much smaller than the first layer. This is also viewed by the density profiles in the growth direction in Fig. 10. Here, the structure is divided into slices of 0.5 nm in the growth direction, and the density is calculated by counting the atomic masses for each slice resulting in a density profile. While the density does not change up to a height of about 14 nm, the range up to 19 nm for the 0° deposition shows a higher increase of the density than 30° and 50° due to filling the open pores with material from the second layer. The impact depth of material from the second layer can be considered to be about 5 nm. However, because the simulated structures are small compared to the experimental ones, resulting in smaller columns widths, the impact depth in the experiment is probably higher. The same initial structure reduces the high fluctuation in density seen for regions above 19 nm, therefore here the higher density can be considered significant, as also supported by the similar initial density for 30° and 50°, which is lost for 19 nm and above. For this region, the density grows by about 0.4 g/cm^3 while fluctuating by a non-negligible amount on the overall growth, but with no significant difference between the second layers.

Due to the structure morphology, an anisotropy for the first layer is expected and confirmed in the following by performing an anisotropic

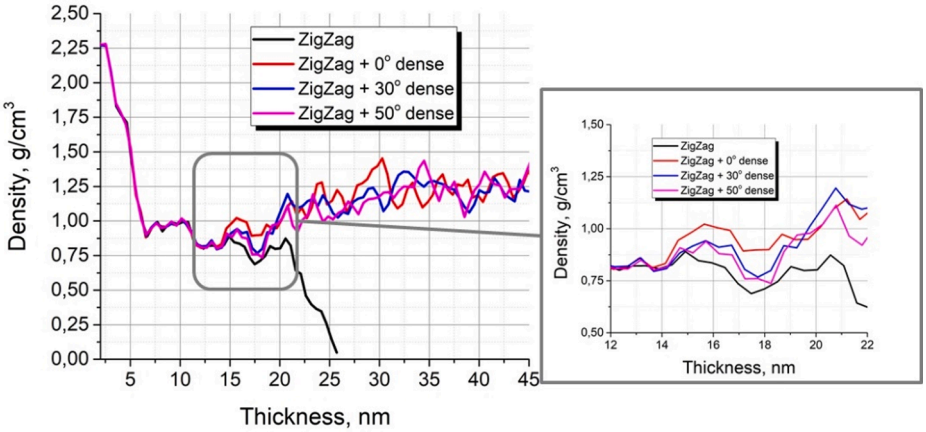

Fig. 10. Density profiles of anisotropic zig-zag single layer and its continuation with dense layers deposited with constant rotation at $\chi = 0°$, 30° and 50°

Table 1
Results of the anisotropic effective medium approximation analysis for the first layer, i.e. the structure height region between 7 and 20 nm, with the impact of the second layer. The uncertainty for the volume distribution is below ±3.6%, while for the birefringence Δn the uncertainty is about ±0.0017 for a 95% confidence interval (see also [26]).

	ZigZag	ZigZag + 0°	ZigZag + 30°	ZigZag + 50°
Volume distribution: material, pores	43.0%,57.0%	46.6%,53.4%	45.2%,54.8%	44.8%,55.2%
Refractive index of fast and slow axis	1.1925,1.2080	1.2128,1.2251	1.2055,1.2184	1.2029,1.2166
Δn	0.0155	0.0123	0.0129	0.0137
Normalized phase retardance @ 266 nm	0.0207°/nm	0.0167°/nm	0.0176°/nm	0.0185°/nm

effective medium approximation analysis as described in [25]. The results are viewed in Table 1 for a bulk refractive index of 1.5 for silica (at 266 nm). The distribution between the filled volume and pores is determined by dividing the structure into voxels of 0.2^3 nm^3. The voxels containing atoms contribute to the filled volume, while empty voxels contribute to the pores. The analysis of the first layer is taken for the growth height region of 7–20 nm, therefore excludes the substrate structure and upper surface region of the first layer but includes the height region impacted by the second layer. For this region, corresponding to the highest porosity, the highest birefringence for normal light incidence is observed for the solely first layer of $\Delta n = 0.0155$. Adding the second layer, the porosity decreases, which also leads to a rise in the value of the refractive index ellipsoid. However, due to the non-directional deposition of the second layer the birefringence decreases to 0.0123 for 0° and increasing again for larger deposition angles of 30° and 50° with 0.0129 and 0.0137, respectively, where the impact on the first layer is decreasing. The birefringence, i.e., the difference of the refractive indices of the slow and fast axis, mainly resembles the refractive index ellipsoid in x and y, because the ellipsoid is nearly aligned with the coordinate axes. The uncertainties for a 95% confidence interval are given in the caption of Table 1, however due to the small number of samples, these are probably overestimated [26].

Repeating the analysis for the growth height region between 25 nm and 47 nm (presented in Table 2), the results show a significantly lower amount of pores in the material. Because this region does not exist prior to the second layer, the influence of the first layer can only be indirect. With a lower number of pores, the refractive indices increase. The birefringence is much lower compared with the region between 7 and 20 nm. In general, for the second layer, a $\Delta n = 0$ can be expected so that the small values can be related to indirect effects from the first layer and/or statistical inaccuracies due to the limited simulated structure size in all dimensions.

Simulated nanostructures are also compared with experimental data and the same conclusions were found: deposition of dense coatings at 30° results in maintaining a more original anisotropy. Columns in simulated zig-zag are thinner than in the experiment, however also the coating thickness (15 nm mean height (~18 nm max)) is much less than in experiments, so columns probably have not fully joined. But within the periodicity of the simulation, the two columns already start joining. Also, the phase retardance of the simulation is by a factor of about 2 lower than in the experiment. Again, the thickness in the simulation is much lower (13 nm) than in the experiment with the smallest thickness (50 nm) – the coalescence of columns is not observed.

The deposition of dense silica thin films on top of porous layers influences the optical anisotropy of the first film. Birefringence is reduced in films with columnar structure when deposition of dense layer is performed at 0° angle and, therefore, the deposition of a dense coating at angles of 30° and 50° with rotating substrate around the normal axis were tested. The investigation was focused on the structural and optical analysis of the single layers, deposited at different angles and with different thicknesses. Afterward, different methods for over coating the porous anisotropic layer was tested. Since the changes of the structure at the interface between two distinct nanostructures is relatively small and difficult to analyze quantitatively, only the changes in optical performance, namely transmission and phase retardance, were measured. Nevertheless, optical measurements were targeted to measure the anisotropic properties – changes in transmission spectra and difference in phase delay for perpendicular polarizations at 0° angle of incidence. In all multi-layer samples, the anisotropic films were deposited at the same conditions, therefore, any changes in optical properties are attributed to the changes in porous layers nanostructure. In order to confirm this hypothesis, molecular dynamic simulations were performed. Results confirmed that different deposition conditions of dense layer influence the nanostructure of the porous layer and its optical anisotropy. Comparison between simulated refractive index differences for fast and slow directions between porous anisotropic and dense layers show similarities with transmission measurements of multilayer coatings. Differences are larger when dense layers are coated at 0° angle due to lower density of thin films deposited at 30° angle. At the same time, simulated birefringence of anisotropic film is larger when dense layer is coated at 30° angle, which explains the increased spectral difference of multilayer, consisted of porous anisotropic and dense isotropic layers coated at 70° and 30° angles, respectively.

Experimental results are limited to anisotropic SiO_2 films, deposited at 70°, but the same principles can be applied to other type of structures, namely columns with different nanostructure, chiral thin films, etc. Also, deposition of different materials by GLAD method may also lead to smaller cracks throughout nanostructured thin films surface. Depending on the size and number of cracks, lower deposition angles can be used for dense thin film formation.

Further research efforts are needed to simulate larger structures in order to compare them directly with experimental results, and investigations with other materials and nanostructures should be continued. We believe that we reported an investigation that can be reproduced with other known materials and nanostructures used in multi-layer optical coatings, thus expanding the capabilities of nanostructured thin films to be used in high performance optical components. Presented results can directly be applied for manufacturing coating-based advanced components such as zero-order waveplates and polarizers for zero angle of incidence, since remaining the anisotropic properties in the porous layer is essential. Also, interface analysis could be used in recently developed all-silica based interference coatings for

Table 2
Results of the anisotropic effective medium approximation analysis for the second layer, i.e. the structure height region between 25 nm and 47 nm. Here, the uncertainty for the volume distribution is below ± 6.8%, while for the birefringence Δn the uncertainty is below ± 0.0077 for a 95% confidence interval (see also [26]).

	ZigZag	ZigZag + 0°	ZigZag + 30°	ZigZag + 50°
Volume distribution: material, pores	–	63.3%,36.7%	61.8%,38.2%	62.0%,38.0%
Refractive index of fast and slow axis	–	1.3037,1.3078	1.2956,1.3002	1.2979,1.2999
Δn	–	0.0041	0.0046	0.0020
Normalized phase retardance @ 266 nm	–	0.0055°/nm	0.0063°/nm	0.0026°/nm

high-power lasers. Overall, any thin film based system, where strict interface is beneficial, could be improved by presented research.

5. Conclusion

In this work, the analysis of optical and structural properties of anisotropic silica thin films is presented, and the technology for maintaining such initial properties in multi-layer coatings when using dense layers is demonstrated. The largest anisotropy was obtained when the substrate was tilted at 70° angle. Phase retardation of such thin films changes during growth from 0.025°/nm to 0.038°/nm at thicknesses of 50 nm and 1500 nm, respectively. Such inhomogeneity of optical retardance is due to changes in films nanostructure: decreasing surface filling and expansion of cracks, which results in increased size of columns with elliptic cross-section during bundling effect. Experimental results indicate that in order to fully exploit such optical anisotropic properties of nanostructured silica thin films in multi-layer coatings, dense layers have to be deposited at 30° angle. Spectrophotometric and ellipsometric data show improved differences in optical response for perpendicular linear polarizations compared with multi-layers containing conventional dense films deposited at 0°. Molecular dynamics simulations of the thin film growth indicate that such behavior is caused by deeper penetration of vapor flux within the porous film in case of dense layer deposition at 0° angle. Therefore, the porosity and the birefringence of the anisotropic layers are reduced. Deposition at 30° angle, on the other hand, maintains a more original anisotropy.

Credit author statement

L. Grineviciute and T. Tolenis designed and carried out the experiments and measurements, H. Badorreck, L. Jensen, D. Ristau and M. Jupé performed the simulations and provided theoretical analysis. Algirdas Selskis performed SEM measurements. All authors participated in discussions, prepared and reviewed the manuscript.

Declaration of Competing Interest

The authors declare that they have no known competing financial interests or personal relationships that could have appeared to influence the work reported in this paper.

Acknowledgements

The authors thank the Deutsche Forschungsgemeinschaft (DFG) for funding within the cluster of excellence PhoenixD (390833453, EXC 2122).

Research also received funding from the Research Council of Lithuania (LMTLT), project UnCoatPower (agreement No S-MIP-20-61).

Appendix A. Supplementary material

Supplementary data to this article can be found online at https://doi.org/10.1016/j.apsusc.2021.150167.

References

[1] A.M. Urbas, Z. Jacob, L.D. Negro, N. Engheta, A.D. Boardman, P. Egan, A. B. Khanikaev, V. Menon, M. Ferrera, N. Kinsey, C. DeVault, J. Kim, V. Shalaev, A. Boltasseva, J. Valentine, C. Pfeiffer, A. Grbic, E. Narimanov, L. Zhu, S. Fan, A. Alù, E. Poutrina, N.M. Litchinitser, M.A. Noginov, K.F. MacDonald, E. Plum, X. Liu, P.F. Nealey, C.R. Kagan, C.B. Murray, D.A. Pawlak, I.I. Smolyaninov, V. N. Smolyaninova, D. Chanda, Roadmap on optical metamaterials, J. Opt. 18 (2016), 093005, https://doi.org/10.1088/2040-8978/18/9/093005.

[2] M. Coll, J. Fontcuberta, M. Althammer, M. Bibes, H. Boschker, A. Calleja, G. Cheng, M. Cuoco, R. Dittmann, B. Dkhil, I. El Baggari, M. Fanciulli, I. Fina, E. Fortunato, C. Frontera, S. Fujita, V. Garcia, S.T.B. Goennenwein, C.-G. Granqvist, J. Grollier, R. Gross, A. Hagfeldt, G. Herranz, K. Hono, E. Houwman, M. Huijben, A. Kalaboukhov, D.J. Keeble, G. Koster, L.F. Kourkoutis, J. Levy, M. Lira-Cantu, J. L. MacManus-Driscoll, J. Mannhart, R. Martins, S. Menzel, T. Mikolajick, M. Napari, M.D. Nguyen, G. Niklasson, C. Paillard, S. Panigrahi, G. Rijnders, F. Sánchez, P. Sanchis, S. Sanna, D.G. Schlom, U. Schroeder, K.M. Shen, A. Siemon, M. Spreitzer, H. Sukegawa, R. Tamayo, J. van den Brink, N. Pryds, F.M. Granozio, Towards Oxide Electronics: a Roadmap, Appl. Surf. Sci. 482 (2019) 1–93, https://doi.org/10.1016/j.apsusc.2019.03.312.

[3] D.T. Reid, C.M. Heyl, R.R. Thomson, R. Trebino, G. Steinmeyer, H.H. Fielding, R. Holzwarth, Z. Zhang, P. Del'Haye, T. Südmeyer, G. Mourou, T. Tajima, D. Faccio, F.J.M. Harren, G. Cerullo, Roadmap on ultrafast optics, J. Opt. 18 (2016), https://doi.org/10.1088/2040-8978/18/9/093006.

[4] R. Messier, T. Gehrke, C. Frankel, V.C. Venugopal, W. Otaño, A. Lakhtakia, Engineered sculptured nematic thin films, J. Vacuum Sci. Technol. A: Vacuum Surf. Films 15 (1997) 2148–2152, https://doi.org/10.1116/1.580621.

[5] K. Robbie, M.J. Brett, A. Lakhtakia, First thin film realization of a helicoidal bianisotropic medium, J. Vacuum Sci. Technol. A: Vacuum Surf. Films 13 (1995) 2991–2993, https://doi.org/10.1116/1.579626.

[6] M. Faryad, A. Lakhtakia, The circular Bragg phenomenon, Adv. Opt. Photon. 6 (2014) 225, https://doi.org/10.1364/AOP.6.000225.

[7] T. Motohiro, Y. Taga, Thin film retardation plate by oblique deposition, Appl. Opt. 28 (1989) 2466, https://doi.org/10.1364/AO.28.002466.

[8] L. Grinevičiūtė, M. Andrulevičius, A. Melninkaitis, R. Buzelis, A. Selskis, A. Lazauskas, T. Tolenis, Highly resistant zero-order waveplates based on all-silica multilayer coatings, Phys. Status Solidi A 214 (2017) 1700764, https://doi.org/10.1002/pssa.201700764.

[9] J.-Q. Xi, M.F. Schubert, J.K. Kim, E.F. Schubert, M. Chen, S.-Y. Lin, W. Liu, J. A. Smart, Optical thin-film materials with low refractive index for broadband elimination of Fresnel reflection, Nature Photon. 1 (2007) 176–179, https://doi.org/10.1038/nphoton.2007.26.

[10] T. Tolenis, L. Grinevičiūtė, R. Buzelis, L. Smalakys, E. Pupka, S. Melnikas, A. Selskis, R. Drazdys, A. Melninkaitis, Sculptured anti-reflection coatings for high power lasers, Opt. Mater. Express. 7 (2017) 1249, https://doi.org/10.1364/OME.7.001249.

[11] P.D. McAtee, A. Lakhtakia, Reflection and transmission of obliquely incident light by chiral sculptured thin films fabricated using asymmetric serial-bideposition technique, J. Nanophoton. 11 (2017), 043502, https://doi.org/10.1117/1.JNP.11.043502.

[12] M. Oliva-Ramirez, A. Barranco, M. Löffler, F. Yubero, A.R. González-Elipe, Optofluidic Modulation of Self-Associated Nanostructural Units Forming Planar Bragg Microcavities, ACS Nano 10 (2016) 1256–1264, https://doi.org/10.1021/acsnano.5b06625.

[13] M. Oliva-Ramirez, J. Gil-Rostra, M.C. López-Santos, A.R. González-Elipe, F. Yubero, Vapor and liquid optical monitoring with sculptured Bragg microcavities, J. Nanophotonics 11 (2017) 1, https://doi.org/10.1117/1.JNP.11.046009.

[14] M. Oliva-Ramírez, J. Gil-Rostra, A.C. Simonsen, F. Yubero, A.R. González-Elipe, Dye giant absorption and light confinement effects in porous bragg microcavities, ACS Photonics 5 (2018) 984–991, https://doi.org/10.1021/acsphotonics.7b01283.

[15] T. Tolenis, L. Grinevičiūtė, L. Smalakys, M. Ščiuka, R. Drazdys, L. Mažulė, R. Buzelis, A. Melninkaitis, Next generation highly resistant mirrors featuring all-silica layers, Sci. Rep. 7 (2017) 10898, https://doi.org/10.1038/s41598-017-11275-0.

[16] S. Macnally, C. Smith, J. Spaulding, J. Foster, J.B. Oliver, Glancing-angle–deposited silica films for ultraviolet wave plates, Appl. Opt. 59 (2020) A155–A161, https://doi.org/10.1364/AO.59.00A155.

[17] I. Hodgkinson, Q. Hong Wu, Serial bideposition of anisotropic thin films with enhanced linear birefringence, Appl. Opt. 38 (1999) 3621, https://doi.org/10.1364/AO.38.003621.

[18] Thin film software: https://www.optilayer.com/, OptiLayer GmbH, n.d. https://www.optilayer.com/.

[19] H. Vankranenburg, C. Lodder, Tailoring growth and local composition by oblique-incidence deposition: a review and new experimental data, Mater. Sci. Eng.: R: Rep. 11 (1994) 295–354, https://doi.org/10.1016/0927-796X(94)90021-3.

[20] C. Smith, S. MacNally, J.B. Oliver, Ellipsometric modeling of serially bi-deposited glancing-angle-deposition coatings, Appl. Opt. 59 (2020) A26, https://doi.org/10.1364/AO.59.000A26.

[21] S. Zhang, X. Zhang, H. Peng, L. Wen, G. Qiu, M. Hu, C. Bai, Structure Analysis of CaO–SiO2–Al2O3–TiO2 Slag by Molecular Dynamics Simulation and FT-IR Spectroscopy, ISIJ Int. 54 (2014) 734–742, https://doi.org/10.2355/isijinternational.54.734.

[22] S. Plimpton, Fast Parallel Algorithms for Short-Range Molecular Dynamics, J. Comput. Phys. 117 (1995) 1–19, https://doi.org/10.1006/jcph.1995.1039.

[23] W.M. Brown, A. Kohlmeyer, S.J. Plimpton, A.N. Tharrington, Implementing molecular dynamics on hybrid high performance computers – Particle–particle particle-mesh, Comput. Phys. Commun. 183 (2012) 449–459, https://doi.org/10.1016/j.cpc.2011.10.012.

[24] W. Humphrey, A. Dalke, K. Schulten, VMD – Visual Molecular Dynamics, J. Molec. Graphics 14 (1996). http://www.ks.uiuc.edu/Research/vmd/,.

[25] H. Badorreck, M. Steinecke, L. Jensen, D. Ristau, M. Jupé, J. Müller, R. Tonneau, P. Moskovkin, S. Lucas, A. Pflug, L. Grinevičiūtė, A. Selskis, T. Tolenis, Correlation of structural and optical properties using virtual materials analysis, Opt. Express. 27 (2019) 22209, https://doi.org/10.1364/OE.27.022209.

[26] H. Badorreck, L. Jensen, D. Ristau, M. Jupé, Statistical analysis on the structural size of simulated thin film growth with molecular dynamics for glancing angle incidence deposition, Coatings 11 (2021), https://doi.org/10.3390/coatings11040469.